



Article

Advanced Rheological, Dynamic Mechanical and Thermal Characterization of Phase-Separation Behavior of PLA/PCL Blends

Evgeni Ivanov * , Rumiana Kotsilkova , Vladimir Georgiev , Todor Batakliiev and Verislav Angelov

Open Laboratory on Experimental Micro and Nano Mechanics (OLEM), Institute of Mechanics, Bulgarian Academy of Sciences, Acad. G. Bonchev Str. Block 4, 1113 Sofia, Bulgaria; kotsilkova@imbm.bas.bg (R.K.); vgeorgiev@imbm.bas.bg (V.G.); batakliiev@imbm.bas.bg (T.B.); v.angelov@imbm.bas.bg (V.A.)

* Correspondence: ivanov_evgeni@imbm.bas.bg; Tel.: +359-29796481

Abstract: This research presents a comprehensive investigation of PLA/PCL polymer blends using advanced rheological characterization, scanning electron microscopy (SEM), differential scanning calorimetry (DSC), and dynamic mechanical, thermal analysis (DMTA) to evaluate phase-separation behavior and functional properties. Polymer composites with various PLA/PCL ratios were fabricated via melt extrusion, a sustainable and scalable approach. The rheological studies revealed significant insights into the blends' viscoelastic behavior, while SEM analyses provided detailed observations of microstructural phase separation. Thermal transitions and crystallization behaviors were evaluated through DSC, and the dynamic mechanical properties were examined via DMTA. The results confirmed that the tailored PLA/PCL blends exhibit properties suitable for advanced additive manufacturing (AM) and shape memory applications, merging flexibility and environmental sustainability. This study emphasizes the novelty of integrating multidisciplinary characterization methods to unravel the structure–property relationships in PLA/PCL systems. By addressing modern demands for eco-friendly, high-performance materials, this work establishes a foundation for the development of innovative polymer composites with potential applications in smart and responsive technologies.

Keywords: PLA/PCL blends; biodegradable polymers; phase separation; rheology; dynamic mechanical; thermal analysis; thermal transitions; crystallinity; thermal stability



Academic Editor: Steven Y. Liang

Received: 26 December 2024

Revised: 17 January 2025

Accepted: 25 January 2025

Published: 27 January 2025

Citation: Ivanov, E.; Kotsilkova, R.; Georgiev, V.; Batakliiev, T.; Angelov, V. Advanced Rheological, Dynamic Mechanical and Thermal Characterization of Phase-Separation Behavior of PLA/PCL Blends. *J. Manuf. Mater. Process.* **2025**, *9*, 35. <https://doi.org/10.3390/jmmp9020035>

Copyright: © 2025 by the authors. Licensee MDPI, Basel, Switzerland. This article is an open access article distributed under the terms and conditions of the Creative Commons Attribution (CC BY) license (<https://creativecommons.org/licenses/by/4.0/>).

1. Introduction

Biodegradable polymers such as polylactic acid (PLA) and polycaprolactone (PCL) have emerged as promising materials for sustainable and environmentally friendly applications due to their biocompatibility, biodegradability, and mechanical versatility. PLA, derived from renewable resources, is known for its rigidity, excellent tensile strength, and biodegradability, making it ideal for various applications, including packaging and biomedical implants [1–6]. However, PLA's inherent brittleness and poor thermal stability limit its broader applicability. In contrast, PCL, with its superior flexibility, lower melting point, and excellent thermal stability, serves as a complementary polymer to PLA. Blending PLA and PCL offers an opportunity to overcome the limitations of each polymer while enhancing the overall material performance [7–17].

The immiscibility of PLA and PCL typically results in phase separation, which significantly influences the mechanical, rheological, and thermal properties of the blends.

Previous studies have reported that phase morphologies such as droplet-matrix, co-continuous, and phase-inverted structures depend on the PLA/PCL ratio and processing conditions [10,18]. The PLA/PCL blend typically exhibits a sea-island morphology, where PCL droplets are dispersed within a continuous PLA matrix. This morphology can transition to a co-continuous structure depending on the ratio of PLA to PCL and the processing conditions. For instance, Urquijo et al. [18] noted that the presence of clay in the PCL phase increases its viscosity, which can inhibit the fracture of PCL domains during processing, leading to the formation of co-continuous structures instead of discrete droplets. Similarly, Solechan et al. [10] demonstrated that varying PCL concentrations in the blend alters the phase morphology, with higher PCL content resulting in distinct dispersed phase morphologies [10]. Researchers have used techniques such as scanning electron microscopy (SEM) to analyze microstructural features and phase separation in these blends. Dynamic mechanical, thermal analysis (DMTA) and differential scanning calorimetry (DSC) have been employed to evaluate the blends' viscoelastic behavior, glass transition temperature (T_g), crystallization behavior, and thermal transitions [19–24].

Rheological properties have also been extensively studied to understand the flow behavior and phase interactions in PLA/PCL blends. Rheological analysis provides insights into the molecular interactions at the interface, shear-thinning behavior, and the extent of phase separation. Studies have shown that increasing the PCL content can suppress PLA crystallization while enhancing the crystallinity of the PCL phase. Additionally, thermal analysis techniques, including thermogravimetric analysis (TGA), have revealed the improved thermal stability of PLA/PCL blends, particularly at low PCL concentrations [21,22,24]. Wachirahuttapong et al. [25] investigated the effects of PCL on morphology, crystallization behavior, and mechanical properties of PLA/PCL blends in the presence of Pluronic as a plasticizer. They found that PLA and PCL are immiscible, with PCL forming droplets within the PLA matrix and their size increasing with higher PCL content. The addition of Pluronic led to improving ductility and elongation at break, but higher concentrations negatively impact mechanical properties due to larger PCL particles. The crystallization behavior of PLA was altered by both PCL and Pluronic. Bouakaz et al. [26] explored the use of organomontmorillonites (Cloisite[®]15A and Cloisite[®]30B) combined with epoxy-functionalized graphene to enhance the compatibility of a PLA/PCL blend. The study demonstrated significant improvements in thermal and barrier properties due to the synergistic effect of these nanofillers. The effectiveness of combining classical melt blending techniques with advanced filler combinations for creating high-performance biodegradable composites was highlighted. In the comprehensive review, Matumba et al. [27] examined the morphological, mechanical, and thermal characteristics of PLA/PCL blends, highlighting the roles of various fillers and compatibilizers in optimizing these properties for diverse applications in packaging, biomedical, and industrial fields.

While existing studies provide valuable insights into the structure–property relationships of PLA/PCL blends, significant gaps remain in understanding the combined effects of blend composition, phase separation, and extrusion processing on their viscoelastic, thermal, and thermomechanical properties. Most previous research has focused on isolated aspects of these properties without fully integrating multiple advanced characterization techniques into a cohesive investigation.

This study presents a comprehensive and multidisciplinary investigation of PLA/PCL blends, integrating advanced rheological characterization, SEM, DSC, TGA, and DMTA techniques. The novelty lies in the systematic analysis of the effects of varying PLA/PCL ratios on phase separation behavior, thermal transitions, crystallization behavior, and viscoelastic properties. Additionally, the study utilizes melt mixing as a sustainable and scalable processing approach, making it highly relevant for industrial applications. The

findings provide deeper insights into the structure–property relationships, enabling the design of PLA/PCL blends tailored for advanced shape memory and additive manufacturing applications. This research bridges the existing knowledge gaps by offering a holistic understanding of the interplay between composition, morphology, and thermal–mechanical properties, contributing to the development of innovative and environmentally sustainable polymer materials.

2. Materials and Methods

2.1. Materials and Processing of PLA/PCL Blends

Two biopolymers, polylactic acid (PLA) Ingeo™ 3D870 (NatureWorks LLC, Plymouth, MN, USA), with a molecular weight of 110,000 g/mol with MFR 9–15 g/10 min at 210 °C/2.16 kg, and polycaprolactone (PCL) from Sigma Aldrich (St. Louis, MO, USA), with molecular weight 80,000 g/mol with MFI 2–4 g/10 min at 160 °C/2.16 kg, were used in pellet form. The PLA/PCL blend compositions were fabricated by extrusion processing, with PLA as the basis component, increasing the PCL content by 5, 30, 40, and 70 wt.%. The neat PLA and PCL polymers were also melt-processed for comparison. Table 1 summarizes the compositions and labeling of each sample. The PLA and PCL pellets were previously dried in an oven at 80 °C and 40 °C, respectively, for 4 h before melt blending. Appropriate amounts of PLA and PCL pellets were manually mixed in a plastic bag, and then mixtures were melted and compounded in a twin-screw extruder Process 11 (Thermo Scientific, Waltham, MA, USA) at a rotating speed of 150 rpm. The temperature profile of the heating zones with a direction from hopper to die was 130 °C→150 °C→170 °C→180 °C→190 °C→190 °C→190 °C→180 °C. After exiting the nozzle, the extrudate passed into two water baths for cooling at 60 °C and then at 20 °C to produce a filament of diameter 1.75 ± 0.5 mm.

Table 1. Summary of the compositions of PLA/PCL blends and labeling.

Reference	PLA wt. %	PCL wt. %
PLA	100	-
95PLA/5PCL	95	5
70PLA/30PCL	70	30
60PLA/40PCL	60	40
30PLA/70PCL	30	70
PCL	-	100

The test samples for rheological and dynamic mechanical, thermal analysis (DMTA) measurements were prepared by hot pressing the pelletized filament using a Carver 3850 hot press (Carver, Inc., Wabash, IN, USA). For the PLA and PLA/PCL binary blends, the pellets were pressed at 180 °C with a pressure of 1 ton. In contrast, the PCL pellets were pressed at 80 °C with 1 ton of pressure.

2.2. Characterization Methods

2.2.1. Scanning Electron Microscopy

Scanning electron microscopy (SEM) was used to visualize the morphology of the blends. Samples were cut in liquid nitrogen and then gold-coated. SEM images of the cross-section of the filament were taken with the Tabletop SEM HI-ROX SH 4000 (Hirox Europe, Limonest, France) at 15 kV accelerating voltage and 110 mA emission current conditions. Micrographs at different magnifications were taken to provide detailed observation of the microstructural hierarchy and phase separation in blends.

2.2.2. Rheological Measurements

All rheological measurements were conducted using a stress-controlled rheometer (AR G2, TA Instruments, New Castle, DE, USA). A strain sweep test was performed over a strain range of 0.01 to 1000 and a frequency of 1 Hz to determine the linear viscoelastic region (LVR). A frequency sweep test was subsequently carried out at a constant temperature of 190 °C, within the frequency range of 0.1 to 100 rad/s, and a strain of 0.1%, ensuring the measurements were within the LVR. The tests were performed using electrically heated parallel plate (EHP) geometry with a 25 mm diameter and a gap of 1000 microns. Three samples with a thickness of 2 mm and a diameter of 20 mm were measured for each blend and neat polymer, and the average results with a standard error of around $\pm 1.0\%$ were presented herewith.

2.2.3. Dynamic Mechanical, Thermal Analysis

Dynamic mechanical, thermal analysis (DMTA) was conducted in torsion mode using the AR G2 rheometer (TA Instruments, USA), employing a temperature ramp from 30 °C to 110 °C at rates of 3 °C/min and 5 °C/min under airflow. All tests were performed at a frequency of 1 Hz, with the maximum deformation set to 0.1%. The test samples were plates of size 60 × 12 × 2.5 mm, and at least three samples were tested of each composition, presenting here the average results, with a standard error of around $\pm 1\%$ at a confidence level of 95%.

2.2.4. Differential Scanning Calorimetry

Differential scanning calorimetry (DSC) measurements of single polymer and blended samples were performed by Discovery D250 (TA Instruments, USA). The heat effects associated with phase transitions and crystallization processes were investigated as a function of the temperature. The test was performed as a 5–8 mg sample was encapsulated in an aluminous pan, and then it was heated from 0 to 200 °C (first run), followed by a subsequent cooling to 0 °C, with a rate of 10 °C/min in a nitrogen atmosphere. Multiple samples ($n = 3$) were used for each blend composition to ensure reproducibility, and the average results with a standard error below $\pm 1\%$ at a confidence level of 95% were presented here. From the DSC thermogram of heating, the temperatures of glass transition (T_g), cold crystallization (T_{cc}), and melting (T_m), as well as their enthalpies (ΔH_{cc}) and (ΔH_m), were determined, while the melt crystallization temperature (T_c) was determined from the thermogram of cooling. The degree of crystallinity (χ_c %) of the PLA and PCL polymers in their blends was calculated based on the enthalpy values by the following equation [28]:

$$\% \text{ crystallinity } (\chi_c) = \left(\frac{\Delta H_m - \Delta H_{cc}}{\omega \Delta H_0} \right) * 100 (\%), \quad (1)$$

where ΔH_0 is fusion enthalpy (J.g^{-1}), ΔH_{cc} is the cold crystallization enthalpy (J.g^{-1}), and ω is the portion of the polymer in the blend. The melting enthalpy when the crystallinity of the polymer is 100% (ΔH_0) was taken of 93 J.g^{-1} for the PLA [29] and 136 J.g^{-1} for the PCL [30]. This approximate equation (1) can provide information on the crystallinity of the sample, removing the effects due to cold crystallization during the DSC scan.

2.2.5. Thermogravimetric Analysis

Thermogravimetric analysis (TGA) was utilized to detect the thermal degradation process, which is related to the mass loss of the specimen as a function of rising temperature from 20 to 500 °C. The test was conducted with Q50 (TA Instruments, USA). A sample of 10 mg was placed in an open platinum pan and heated with a ramp of 10 °C/min under a nitrogen flow rate of 50 mL/min. Multiple samples ($n = 3$) were tested for each blend

composition, and the average results with a standard error below $\pm 1\%$ were presented here. The decomposition steps and characteristic temperatures corresponding to 2%, 5%, 10%, and 50% weight loss and the decomposition peak temperature (T_p) and the residue ash at 500 °C were evaluated from the TG and DTG thermograms to determine the degree of thermal stability and the degradation of PLA, PCL, and blends.

Figure 1 presents the workflow scheme related to the fabrication, processing, and analysis of PLA/PCL blends for morphological, thermal, and rheological characterization in the current study.

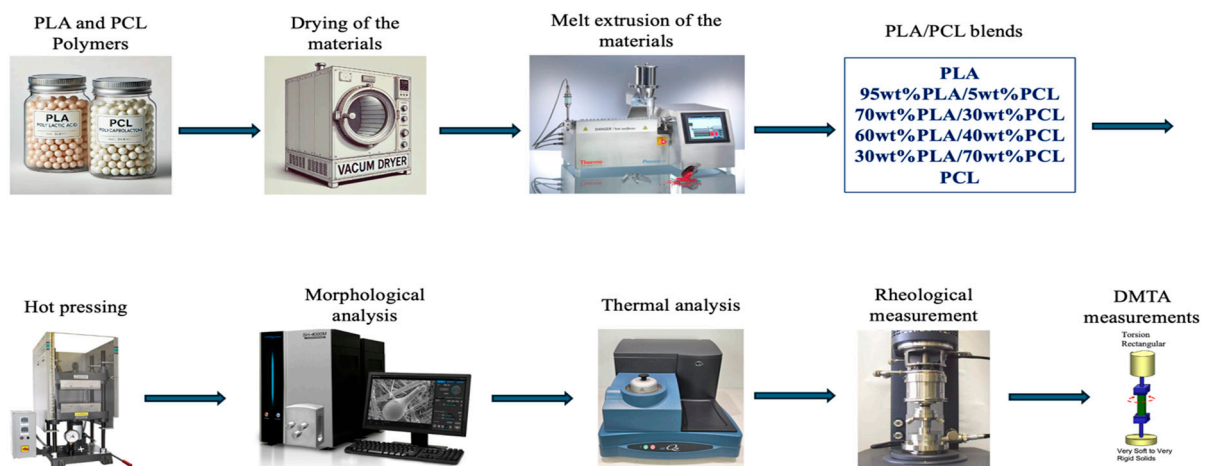


Figure 1. Processing and characterization workflow of PLA/PCL polymer blends.

3. Results and Discussion

3.1. Morphology of PLA/PCL Blends

It is important to start with a description of the microstructure of blends due to its crucial role in the properties. In Figure 2, SEM micrographs of fracture surface morphology of phases with varying ratios of 5/95, 70/30, 60/40, and 30/70 *w/w* PLA/PCL are presented at low and high magnifications. As can be seen, the 95 PLA/5PCL blend formed a sea-island microstructure with a spherical-shaped droplet-matrix morphology of irregular PCL spheres with different dimensions ranging from 0.5 to 1 μm , immersed in the PLA continuous phase. This morphology is indicative of a phase-separated immiscible blend with poor compatibility between PLA and PCL phases [21,31,32]. On the other hand, the 70PLA/30PCL and 60PLA/40PCL blends presented co-continuous phase morphology of each homopolymer with the presence of some irregular spherical droplets of bigger size. Finally, in the 30PLA/70PCL blend, the inversion of phase occurred; thus, small PLA droplets of size $\sim 0.5 \mu\text{m}$ were dispersed in the PCL matrix.

Researchers usually reported [33–36] that PLA/PCL blends with PCL content until 30 wt.% formed typical droplets-in-matrix morphology, while the 40–60 wt.% PCL content resulted in coarse co-continuous morphology. In our study, it is observed that phase inversion from a droplet-like phase to a co-continuous phase occurred at 30 wt% PCL. This might result from differences in viscosity, melting temperature, and crystallinity of both polymers. In a comprehensive review, Fortelny et al. [23] reported that PLA and PCL are immiscible polymers, but their interfacial tension is quite low; hence, PLA/PCL blends with good mechanical properties can be prepared without the addition of a compatibilizer. While mechanical properties were reported to be very sensitive to the blend composition and morphology, the effects on other properties were insufficiently investigated. Therefore, in the present study, we focused on the effects of the blend composition, the crystallinity, and the blend morphology on the viscous, viscoelastic, and thermal behavior of the investigated PLA/PCL blends.

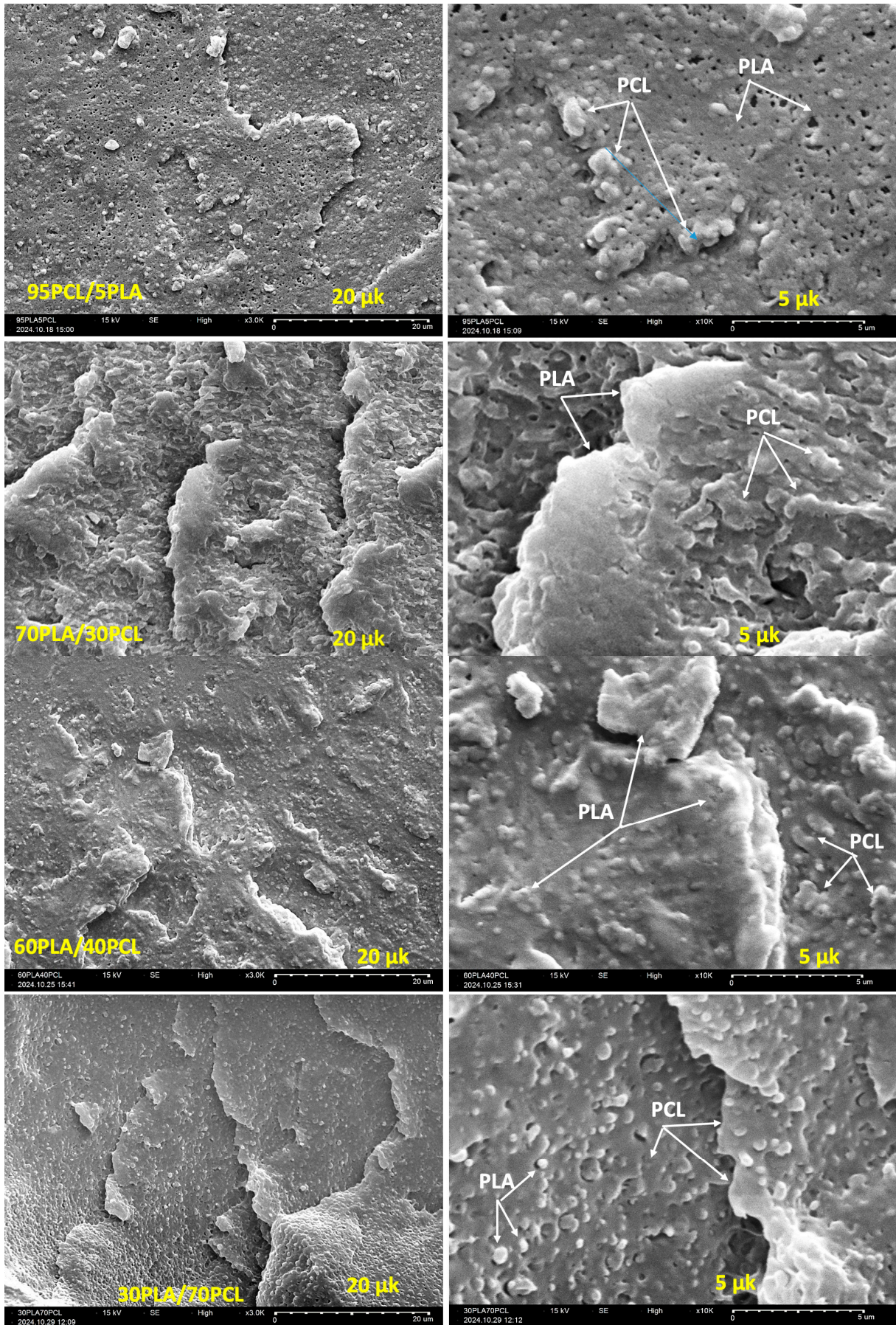


Figure 2. SEM micrographs of blends with ratios of 95/5, 70/30, 60/40, and 30/70 *w/w* PLA/PCL at low and high magnifications of 20 μm and 5 μm. Arrows pointed to the PLA and the PCL phases.

3.2. Rheological Properties

To provide more information regarding the interactions between the immiscible polymers PLA and PCL, a dynamic rheological test was performed. The complex viscosity (η^*), storage (G'), and loss (G'') moduli variations versus angular frequency (ω) were measured at 190 °C. In Figure 3a–f, the results are plotted individually for each sample: the PLA, PCL, and binary blends. In Figure 3g,h, the η^* and G' & G'' are compared for all tested samples.

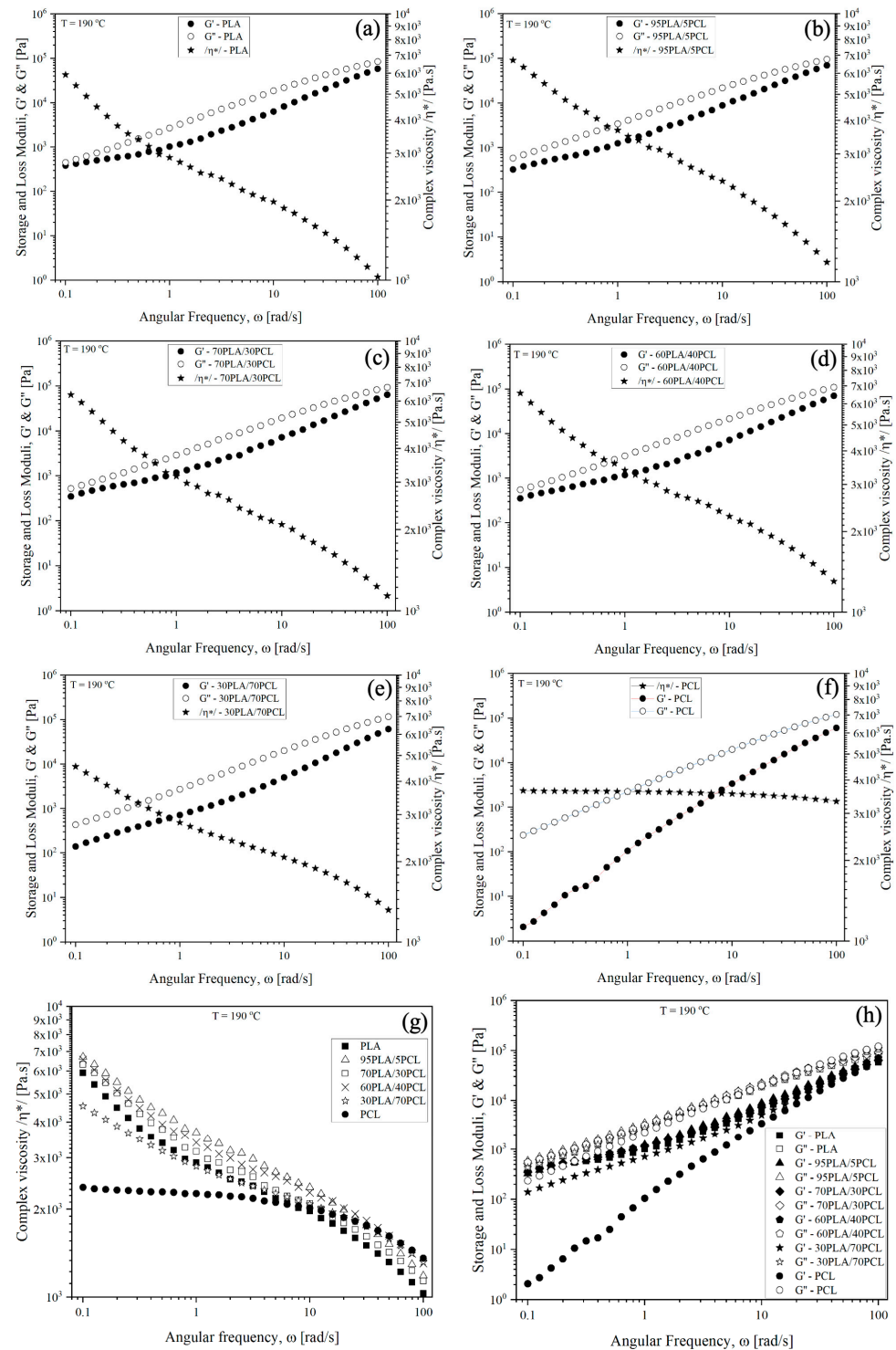


Figure 3. (a–h) Dynamic rheological characteristics, G' & G'' , and η^* vs. angular frequency (ω) of melts at 190 °C: (a) PLA, (b) 95PLA/5PCL, (c) 70PLA/30PCL, (d) 60PLA/40PCL, (e) 30PLA/70PCL, (f) PCL, and (g,h) comparison of η^* and G' & G'' vs. (ω) for all samples at 190 °C.

Considering the complex viscosity in Figure 3a–f, the neat PCL exhibited Newtonian flow behavior at low frequencies with a slight shear thinning behavior at higher frequencies above 10 rad/s. On the other hand, the PLA demonstrated pseudoplastic behavior at low frequencies, a tendency to plateau in the middle range, and a strong shear thinning at high frequencies > 10 rad/s. Moreover, the viscosity of PLA is threefold higher than that of PCL at $\omega \sim 0.1$ rad/s; however, in the shear thinning range, its viscosity becomes lower than that of PCL, which was associated with the different molecular structures of both polymers. Comparing all samples in Figure 3g, the binary blends of 5, 30, and 40 wt.% PCL showed higher viscosity than that of the neat PLA in the entire frequency range, indicating the presence of phase-separated microstructure of immiscible blends and confirming the SEM visualization in Figure 2. On the other hand, the viscosity of the 30PLA/70PCL blend at low frequencies is slightly lower than that of the PLA but twofold higher than that of the PCL, which was associated with the inversion of phases, shown in Figure 2. In general, all binary blends demonstrated strong shear thinning behavior similar to PLA, where at low frequencies around $\omega \geq 0.1$ rad/s, the complex viscosity decreased in the order: 95PLA/5PCL > 60PLA/40PCL > 70PLA/30PCL > PLA > 30PLA/70PCL >> PCL.

An overall observation on the dynamic storage modulus (G') and loss modulus (G'') vs. angular frequency (ω) in Figure 3a–f showed that both dynamic moduli increased as the frequency increased; moreover, the G' and G'' slopes of the PLA and all PLA/PCL blends were lower than those of PCL, which is typical for the viscoelastic liquids. In Figure 3h, a high elasticity contrast between the PLA and PCL polymers is observed ($G'_{\text{PLA}}/G'_{\text{PCL}} = 150$ at $\omega = 0.1$ rad/s) because of the large difference between their glass transitions: ~ 60 °C for PLA and about -60 °C for the PCL. Furthermore, the G' and G'' values of the PLA/PCL blends with 5, 30, and 40 wt.% PCL contents were close to that of the matrix PLA, confirming the low sensitivity to the morphological developments of the PLA/PCL immiscible blends. The storage modulus (G') of the 30PLA/70PCL blend has values much higher than that of the PCL. This phenomenon was related to the yield behavior [36] that may result from a slight cross-linking of the blend structure owing to the phase inversion in the immiscible blend with the PCL major phase. The “cross-linking” refers here to enhanced physical interactions between PLA and PCL phases. Evidence for this includes increased complex viscosity at low frequencies, enhanced storage modulus (G'), and deviations from liquid-like behavior in Cole–Cole plots (Figure 4b), particularly in blends with phase inversion or intermediate PCL content, and these observations reflect network-like structures arising from phase morphology and interfacial interactions.

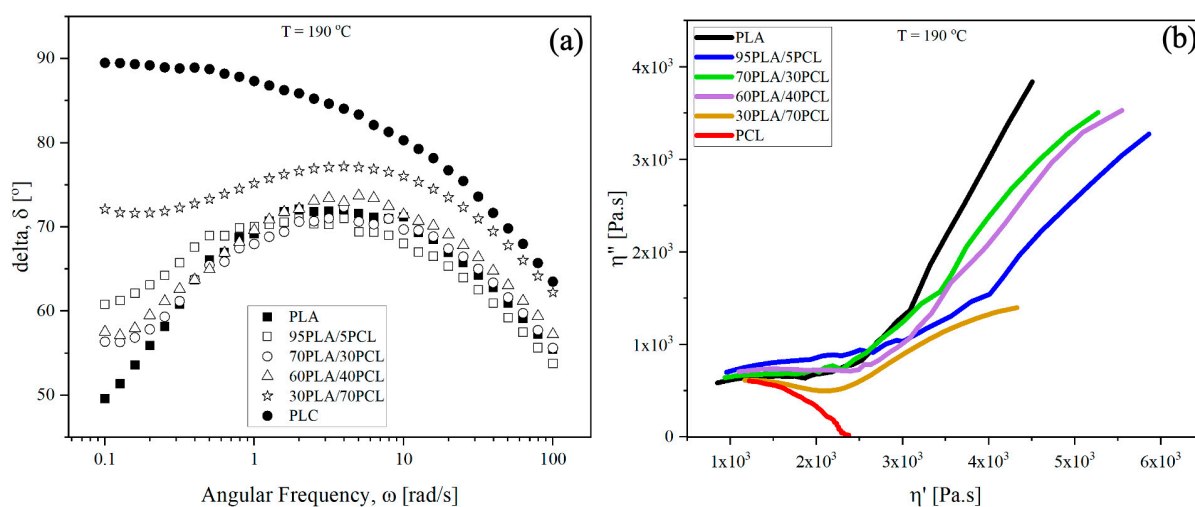


Figure 4. (a,b) Phase angle (δ) as a function of angular frequency (a) and Cole–Cole plots (b) for PCL/PLA blends at various weight ratios at 190 °C.

Figure 4a,b presents (a) the phase angle (δ) as a function of angular frequency (ω), as well as (b) the Cole–Cole plots (η'') vs. (η'), comparing the neat PLA and PCL polymers with the PLA/PCL blends. As shown in Figure 4a, the phase angle (δ) at $\omega = 0.1$ rad/s was found to increase from 50° to 72° for the PLA and the PLA/PCL blends with increasing the PCL contents from 5 to 70 wt.%, which is a typical viscoelastic material's response. While $\delta \sim 90^\circ$ for the neat PCL indicated a Newtonian behavior in the low-frequency range. In Figure 4b, the Cole–Cole plots, presenting the imaginary (η'') vs. real (η') viscosity parts of the complex viscosity, are explored to characterize the effect of composition ratio on the morphological changes in the PCL/PLA blends. In the referred literature [37], it was suggested that two-phase systems with liquid-like behaviors produce a smooth semicircular arc in the Cole–Cole plot, while those with solid-like behavior produce an arc that deviates from the semicircular shape. Comparing our samples in Figure 4b, it was found that the amount of the PCL in the PLA/PCL blends had a significant influence on the shape of its Cole–Cole curves. Thus, for the 95PLA5/PCL blend in the early stages of phase separation, the Cole–Cole curve deviated from the semicircular shape and went straight upward at high viscosity, indicating that the blend behaves like an elastic gel. For other blends, such as 70/30, 60/40, and 30/70 w/w PLA/PCL, the shapes of the Cole–Cole plots became semicircular at high viscosities, indicating a liquid-like behavior where the systems approached the break-up state of the network and forms disconnected domains or droplet-matrix morphology.

Therefore, this rheological analysis provided suitable criteria to differentiate the separation in the two-phase systems. The rheological results from this study will be used in our further works applying mathematical modeling and simulation to predict 3D printing process parameters [38] and the flow instability [39] of PLA/PCL blends and nanocomposites towards the design of 3D printable materials.

3.3. Dynamic Mechanical Thermal Analysis of PLA and PLA/PCL Blends

The results from dynamic mechanical, thermal analysis (DMTA) under airflow for the neat PLA and the PLA/PCL blends with various PCL contents are presented in Figure 5. Figure 5a–e show the temperature dependence of the storage modulus (G') and loss modulus (G'') individually for each sample when comparing two heating rates, $3^\circ\text{C}/\text{min}$ and $5^\circ\text{C}/\text{min}$. The G' indicated the elastic or solid-like behavior, while G'' indicated the viscous or liquid-like behavior of the material. The black curves are for the heating rate of $3^\circ\text{C}/\text{min}$, and the red curves are for the heating rate of $5^\circ\text{C}/\text{min}$. The G' (T) curves showed a clear drop around 70 – 80°C , with a peak for G'' (T) corresponding to the PLA glass transition ($T_{g,PLA}$). At the heating rate of $5^\circ\text{C}/\text{min}$, the ($T_{g,PLA}$) transition occurred at slightly higher temperatures compared to that at $3^\circ\text{C}/\text{min}$. At temperatures above the ($T_{g,PLA}$), the storage moduli strongly decreased in three decades. Some authors [40,41] suggested that the ratio between the glassy state and the rubbery plateau moduli measured in the DMA test can be used to represent the shape memory behavior of materials. Additionally, between 90°C and 110°C , an increase in both moduli was observed because of the cold-crystallization of the PLA phase [42]. Figure 5f,g compares the G' & G'' vs. temperature (T) for the neat PLA and all PLA/PCL blends at heating rates of $3^\circ\text{C}/\text{min}$ (f) and $5^\circ\text{C}/\text{min}$ (g), respectively. Adding 5 wt.% PCL to PLA insufficiently changed the storage modulus (G') at low temperatures but increased the G' drop after the $T_{g,PLA}$ if compared to the neat PLA. This could be related to the presence of sea-island microstructure with small domains of PCL dispersed in the PLA matrix. The blends 70PLA/30PCL and 60PLA/40PCL have similar behavior with twice lower values of both moduli compared to the neat PLA, which was associated with the formation of a co-continuous phase morphology. For the sample 30PLA/70PCL,

the storage and loss moduli showed a further decrease across the entire temperature range, indicating even more dominance of the flexible PCL phase due to phase inversion.

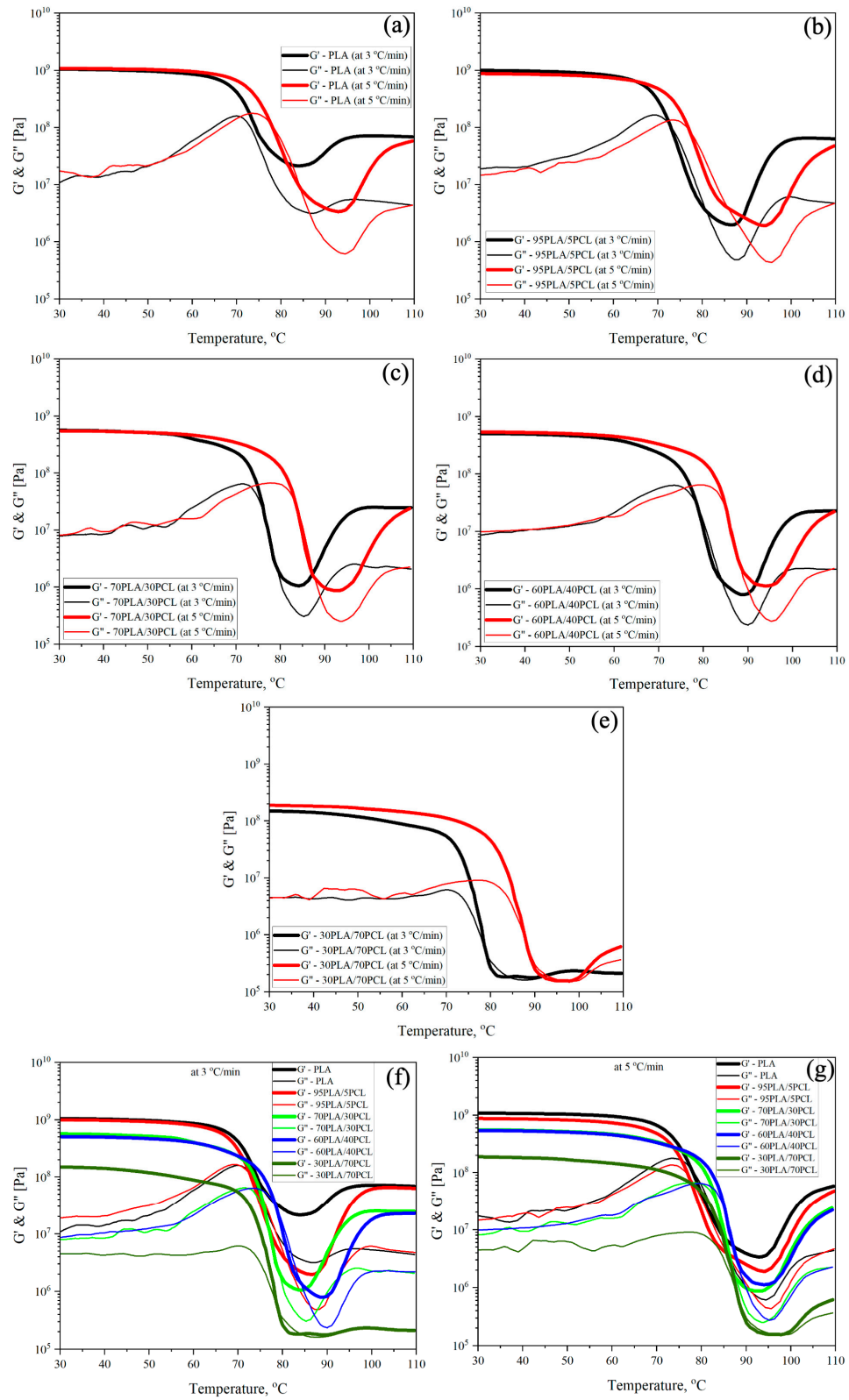


Figure 5. (a–g) Storage and loss moduli (G' & G'') vs. temperature (T) at heating rates of $3\text{ }^{\circ}\text{C}/\text{min}$ and $5\text{ }^{\circ}\text{C}/\text{min}$ under airflow of (a) PLA, (b) 95PLA/5PCL, (c) 70PLA/30PCL, (d) 60PLA/40PCL, (e) 30PLA/70PCL, (f) PCL, and (fg) comparison of G' & G'' vs. T at $3\text{ }^{\circ}\text{C}/\text{min}$ and $5\text{ }^{\circ}\text{C}/\text{min}$, respectively.

The DMTA study highlighted the impacts of the PCL content and the heating rate on the thermal and mechanical behavior of PLA/PCL blends. The decrease in storage modulus (G') by blending PLA with PCL confirmed that the PCL significantly alters the crystallization behavior of PLA [19]. In general, the increase in heating rate from 3 °C/min to 5 °C/min consistently shifted the T_g to higher temperatures for all blends, and the effect was associated with the reduced time available for molecular relaxation during heating. The low content of 5 wt.% PCL produced a minimal effect on the G' modulus and $T_{g,PLA}$ compared to the neat PLA due to the sea-island morphology of small PCL domains dispersed within a continuous PLA matrix. Supporting evidence for this observation is provided by the DSC results (Section 3.4.1), where the melt crystallization temperature of PLA decreases from 103 °C for the neat PLA to 100 °C for the 95PLA/5PCL blend. Additionally, TGA analysis (Section 3.4.2) confirmed a single-step degradation process for this composition. In contrast, the higher PCL content significantly reduced the G' values, broadened the peak of $T_{g,PLA}$, and promoted phase interactions associated with the formation of co-continuous phase morphology at 30 and 40 wt% PCL and phase inversion at 70 wt.% PCL, respectively. The higher amount of PCL strongly suppressed the PLA crystallization, and this was confirmed by the DSC results below (Section 3.4.1), where the melt crystallization of the PLA is not visible at 30–70 wt.% PCL. The reduction in modulus is further influenced by the high degree of PCL crystallinity in the blends and its positive contribution to the thermal degradation profile, as confirmed by the DSC and TGA analyses below.

Figure 6a,b presents the $\tan \delta$ vs. temperature curves comparing the neat PLA and the PLA/PCL blends at two heating rates, 3 °C/min (a) and 5 °C/min (b). $\tan \delta$ represents the ratio of loss modulus (G'') to storage modulus (G'), reflecting the material's damping behavior. In our case, the $\tan \delta$ peak corresponds to the glass transition ($T_{g,PLA}$), where the transition from a glassy state to the rubbery state of the PLA polymer occurs. Blending PLA with PCL resulted in a shift of $\tan \delta$ peaks to higher temperatures and a broadening of the peak as the PCL content increases, demonstrating that the higher PCL content dominates the thermal response of the blends. Comparing the two heating rates in Figure 6a,b, we can conclude that the heating rate of 5 °C/min shifted the $\tan \delta$ peaks to higher temperatures compared to 3 °C/min for all compositions due to kinetic effects during thermal transitions. Broadening of the $\tan \delta$ peak became more pronounced with increasing the PCL content; this was reflected by the changes in phases and more significant phase separation.

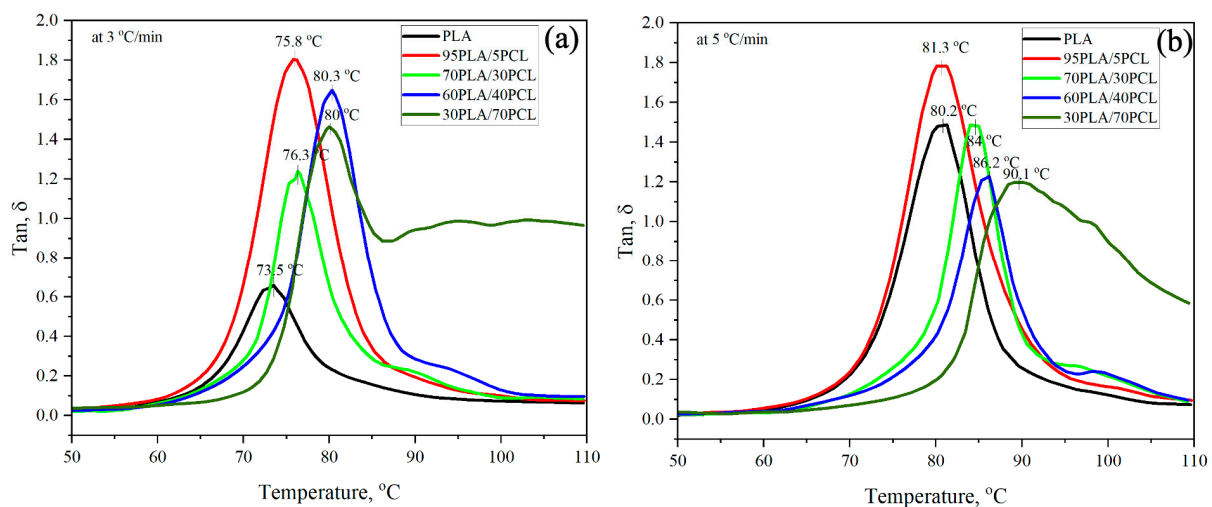


Figure 6. (a,b) $\tan \delta$ curves for the neat PLA and the PLA/PCL blends with increasing the PCL content from 5 to 70 wt.% at heating rates 3 °C/min (a) and 5 °C/min (b).

Figure 7 presents the PLA glass transition temperature ($T_{g,PLA}$) in the blends with varying PCL content, as determined by the DMTA test at two different heating rates: 3 °C/min (black dots) and 5 °C/min (red dots). It can be seen that the $T_{g,PLA}$ is 6–10 °C higher at the higher heating rate of 5 °C/min compared to the 3 °C/min for all compositions. This behavior arises due to kinetic effects that limit molecular relaxation. The faster heating rate reduced the relaxation time needed for the molecular segments to respond, causing the glass transition to occur at higher temperatures. Moreover, as the PLA content decreased in the PLA/PCL blends, the $T_{g,PLA}$ gradually increased for both heating rates. The variation across the blends is small (1–2%) for the 95PLA/5PCL blend compared to the neat PLA, but it increased to 6–8% at 30PLA/70PCL. However, at 5 °C/min, the $T_{g,PLA}$ shows a consistent inverse relationship, with a decreasing percentage of PLA in the blend, which aligns with the expected influence of PCL content and the phase morphology. This trend may be associated with the PCL effects on the segmental dynamics and reduced mobility of PLA chains, likely due to the phase interactions and possible suppression of PLA crystallization, as well as to the formation of phase-separated to co-continuous morphologies, particularly at higher PCL content. Meanwhile, at 3 °C/min, the variations in $T_{g,PLA}$, including apparent outliers, could be influenced by the increased sensitivity to molecular relaxation at a slower heating rate. The slower heating rate allows more time for phase-specific interactions, leading to potential deviations depending on the morphology and crystallinity of individual samples.

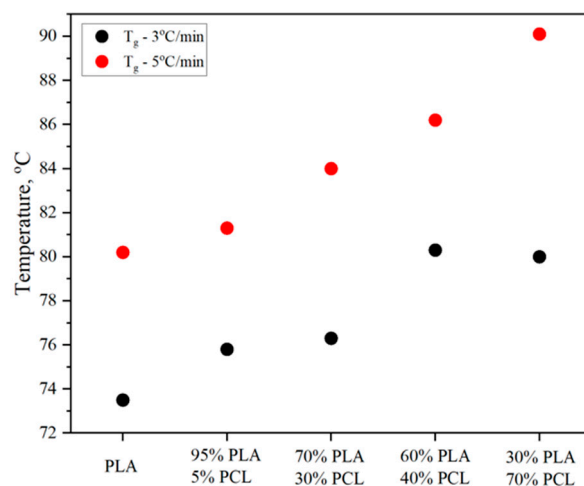


Figure 7. Glass transition temperature ($T_{g,PLA}$) determined from DMTA tests for PLA and its blends with varying PCL content at two different heating rates: 3 °C/min (black dots) and 5 °C/min (red dots).

In Table 2, the $T_{g,PLA}$ values, as determined by DMTA (at two heating rates) and DSC tests (in Section 3.4.1), are compared. The observed difference in the $T_{g,PLA}$ determined by both tests for the neat PLA can be attributed to the distinct physical properties measured by each technique. The DMTA measured mechanical changes in the variations in storage and loss moduli as a response to temperature, while the DSC analysis detected calorimetric changes associated with the heat flow during the glass transition [43–45]. These transitions for one and the same sample were manifested at different temperatures, as affected by the heating rate and the differing sensitivities and principles of the two methods.

Table 2. The glass transition temperature of PLA ($T_{g,PLA}$) in the blends with varying PCL content, as determined by the DMTA and the DSC tests.

Sample	$T_{g,PLA}$ [$^{\circ}C$]		
	DMTA Test at 3 $^{\circ}C/min$	DMTA Test at 5 $^{\circ}C/min$	DSC Test at 10 $^{\circ}C/min$
PLA	73.5	80.2	59.7
95PLA/5PCL	75.8	81.3	not determined *
70PLA/30PCL	76.3	84.0	not determined *
60PLA/40PCL	80.3	86.2	not determined *
30PLA/70PCL	80	90.1	not determined *

* The $T_{g,PLA}$ cannot be determined correctly in the PLA/PCL blends as the melting point of the PCL overlapped with the glass transition of the PLA (see Figure 8a below in Section 3.4.1).

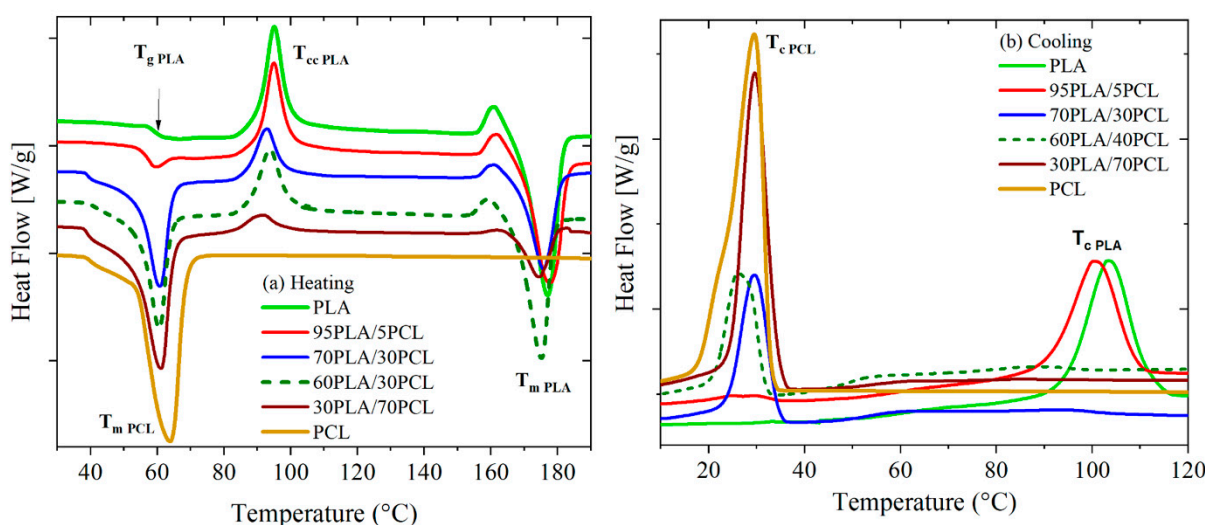


Figure 8. (a,b) DSC thermograms of PLA, PCL, and blends: (a) heating run and (b) cooling run at a ramp of 10 $^{\circ}C/min$.

3.4. Thermal Analyses of PLA/PCL Blends

3.4.1. DSC Evaluation of Phase Separation and Crystallinity of Blends

The effect of PCL amount on the PLA/PCL thermal transitions and crystallization behavior was investigated by DSC analysis. In Figure 8, the DSC curves of heat flow vs. temperature are presented. The thermal and crystallization characteristics are summarized in Table 3. In Figure 8a, the heating thermograms show the glass transition (T_g) of the neat PLA around 60 $^{\circ}C$, followed by the cold crystallization peak at $T_{cc} \sim 95$ $^{\circ}C$ and melting peak at $T_m \sim 177$ $^{\circ}C$. In the thermograms of the PLA/PCL blends, two melting peaks were observed ($T_{m,PCL}$) for the PCL and ($T_{m,PLA}$) for the PLA, which was associated with the phase separation in immiscible polymer blends. The cold crystallization temperature (T_{cc}) and the melting temperature ($T_{m,PLA}$) of the PLA were slightly shifted with 3–5 $^{\circ}C$ to lower temperatures by increasing the PCL content. Furthermore, the glass transition of PLA ($T_{g,PLA}$) overlapped with the melting peak of PCL ($T_{m,PCL}$) in the PLA/PCL blends and cannot be determined, as it was performed with the DMTA tests. The PCL showed only a melting peak ($T_{m,PCL}$) in the temperature region studied. While in the blends, the melting peak of the PCL appeared at slightly lower temperatures (60–61 $^{\circ}C$) compared to the neat PCL (~ 64 $^{\circ}C$).

Table 3. Thermal characteristics of PLA/PCL blends.

Sample	T_g PLA °C	T_m PCL °C	ΔH_m PCL J·g ⁻¹	T_{cc} PLA °C	ΔH_{cc} PLA J·g ⁻¹	T_m PLA °C	ΔH_m PLA J·g ⁻¹	T_c PLA °C	T_c PCL °C	χ_c PLA, %	χ_c PCL %	χ_c Total %
PLA	59.7	-	-	95.0	22.7	177.0	36.0	103.4	-	14.3	-	14.3
95PLA/5PCL	-	59.3	2.5	94.9	19.1	177.5	31.3	100.4	29.4	13.8	36.8	50.6
70PLA/30PCL	-	60.7	27.2	92.7	11.4	175.8	20.1	-	29.5	13.4	66.7	80.1
60PLA/40PCL	-	59.9	25.3	90.1	15.1	175.1	27.5	-	27.8	22.2	46.5	68.7
30PLA/70PCL	-	61.1	38.1	91.7	4.5	174.5	8.5	-	29.6	14.3	40.1	54.4
PCL	-	63.8	58.0	-	-	-	-	-	29.5	-	42.6	42.6

In the cooling thermograms in Figure 8b, a melt crystallization peak of the PLA ($T_{c\text{ PLA}}$) was observed around 103 °C for the neat PLA, and at 100 °C for the 95PLA/5PCL blend. By increasing the PCL content in the blends, the melt crystallization peak of the PLA disappeared, which demonstrated the suppressing effect of PCL on the PLA crystallization. In contrast, a melt crystallization peak of the PCL appeared at 30 °C for the blends containing 30, 40, and 70 wt.% PCL. The variation in crystallization temperature of the PC, $T_{c\text{ PCL}}$ was ~2% across the blends by increasing the PCL content, but the peak intensity was increased, which was associated with the increased amount of crystallized PCL.

The percentage of crystallinity of both phases in the blends was determined from the melting enthalpies using Equation (1). Table 3 summarizes the results. Figure 9 presents the PLA, PCL, and total crystallinity depending on the blend ratio. The PLA crystallinity in the blends is relatively low, around $\chi_{c\text{ PLA}} \sim 14\%$, and it was insufficiently affected by increasing the PCL content with variation across the blends of 2–3%, with the exception of the 60PLA/40PCL blend with $\chi_{c\text{ PLA}} \sim 22\%$. In contrast, a large degree of crystallinity was determined for the PCL in the blends, which is $\chi_{c\text{ PCL}} = 43\%$ for the neat PCL, and it increased to $\chi_{c\text{ PCL}} = 67\%$ with a variation of 30% for the co-continuous blends 70PLA/30PCL. In contrast, the crystallinity of the blends with sea-island morphology decreased to $\chi_{c\text{ PCL}} = 37\text{--}40\%$, compared to the neat PLA with variation across the blends around 5%. Researchers [23,34] found that the optimum size of the PCL particles in the PLA/PCL blends depends on the degree of crystallinity of the PLA when it is a major phase. In our case, the low crystallinity of the PLA ($\chi_{c\text{ PLA}} \sim 14\%$) is probably determining the size of the PCL spheres (0.5–1 μm) in the immiscible blend with sea-island morphology, as observed in Figure 2. Respectively, the much higher crystallinity of PCL ($\chi_{c\text{ PCL}} \sim 43\%$) determined the smaller size ~0.5 μm of the PLA droplet in the 30PLA/70 PCL blend, where the PCL is the major phase.

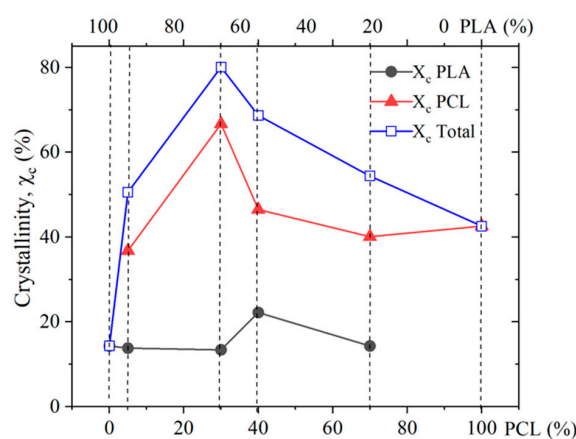


Figure 9. The crystallinity of the PLA, PCL, and total crystallinity depending on the blend ratio.

3.4.2. Thermal Stability and Degradation of PLA/PCL Blends

The TGA was performed to evaluate the thermal stability and degradation of the PLA/PCL blends. Figure 10a compares the thermograms of the weight loss vs. temperature of the neat polymers and the PLA/PCL blends with increasing the PCL content from 5 to 70 wt%. Figure 10b shows the first derivative of the weight loss vs. temperature. As seen, the neat PLA and PCL, as well as the 95PLA/5PCL blend, have only one degradation stage, while the thermal degradation of other PLA/PCL blends occurred in two steps. The first step was related to the PLA decomposition, and the second step was associated with the PCL degradation, which confirmed the phase separation of both polymers in the immiscible PLA/PCL blends.

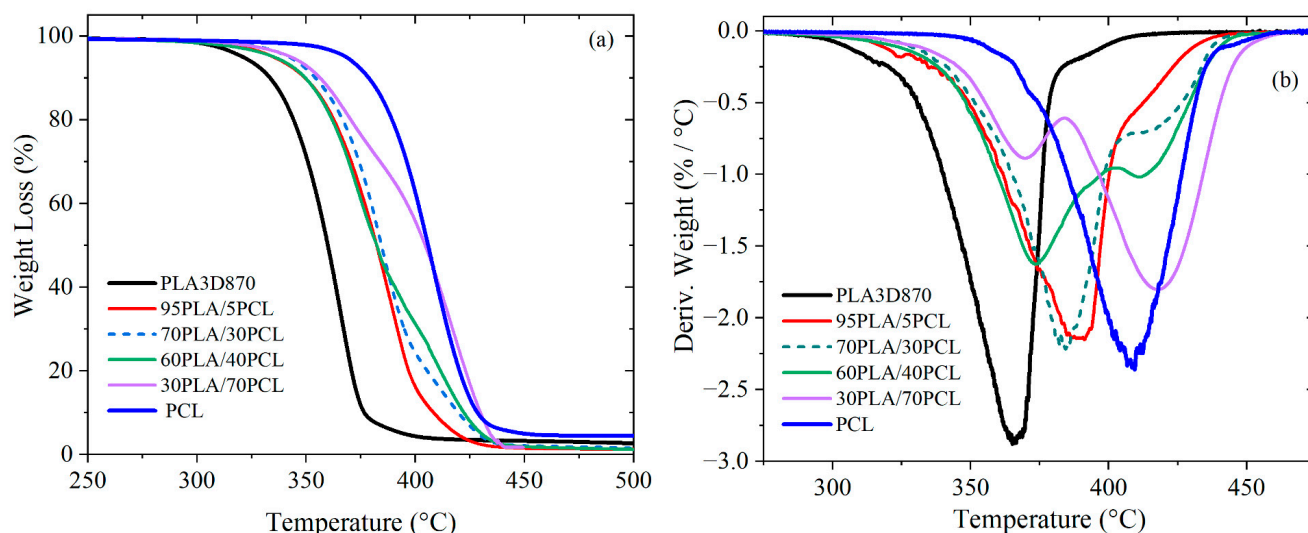


Figure 10. TGA thermograms of weight loss vs. temperature (a) and their first derivative (b) of the PLA/PCL blends.

Figure 11 shows the temperature plots corresponding to the 2%, 5%, 10%, and 50% weight loss, evaluating the degree of thermal stability with increasing the PCL content in the PLA/PCL blends. Additionally, Table 4 summarizes the temperatures of the thermal stability, as well as the degradation peaks of the PLA and PCL in the blends, evaluated by the DTG curves (in Figure 10b). The results showed that the PLA is thermally stable up to 305 °C, while the thermal stability of the PCL is much higher (347 °C). Importantly, the addition of a small amount of 5 wt.% PCL significantly increased the thermal stability of the PLA/PCL blend by 12–15 °C, with a variation of about 3%, while a further increase of PCL content to 70% slightly increased the thermal stability with variation across the blends around 1%. The DTG peak of thermal degradation of the PLA ($T_{\text{DTG peak, PLA}}$) is significantly shifted to higher temperatures by the addition of PCL, and this effect is mostly presented at the low PCL content. In contrast, the peak of thermal degradation of the PCL ($T_{\text{DTG peak, PCL}}$) is insufficiently affected by the composition.

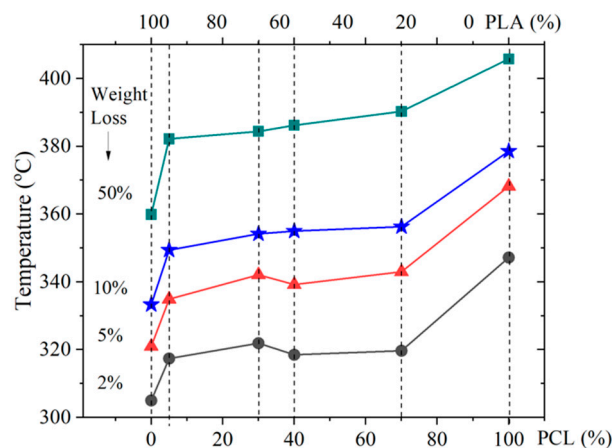


Figure 11. Temperatures corresponding to the 2% (dark green circle), 5% (red triangle), 10% (blue star), and 50% (light green square) weight loss vs. the PCL content in the PLA/PCL.

Table 4. Thermal degradation parameters of PLA/PCL blends.

Sample	T _{-2%} °C	T _{-5%} °C	T _{-10%} °C	T _{-50%} °C	T _{DTG peak, PLA} °C	T _{DTG peak, PCL} °C	R (500 °C) %
PLA	305.0	321.0	333.3	359.9	365.5	-	2.68
95PLA/5PCL	317.4	334.9	349.4	382.2	391.3	-	1.23
70PLA/30PCL	321.9	342.1	354.2	384.4	384.4	412.5	1.47
60PLA/40PCL	308.5	335.2	349.5	382.2	373.2	411.1	1.20
30PLA/70PCL	319.7	343.0	356.3	404.3	369.6	413.4	1.98
PCL	347.2	368.3	378.6	405.8	-	411.7	4.45

4. Conclusions

Scanning electron microscopy (SEM) revealed distinct phase-separation morphologies depending on the PLA/PCL ratio, with sea-island structures at low PCL content, co-continuous morphologies at intermediate ratios, and phase inversion at high PCL content. The rheological analysis demonstrated significant shear-thinning behavior, with blends showing enhanced viscosity and moduli compared to neat PLA and PCL, influenced by phase interactions and blend composition. Dynamic mechanical, thermal analysis (DMTA) indicated that increasing PCL content reduced the storage modulus (G') and shifted the glass transition temperature (T_g) of PLA blends to higher temperatures, with notable effects at higher heating rates. Differential scanning calorimetry (DSC) confirmed that higher PCL content suppressed PLA crystallization while enhancing PCL crystallinity. Thermogravimetric analysis (TGA) demonstrated improved thermal stability in PLA/PCL blends, particularly at low PCL concentrations, with phase separation evident in distinct degradation stages. Collectively, the results indicate that PLA/PCL blends exhibit tunable properties suitable for advanced applications, balancing mechanical flexibility, thermal stability, and environmental sustainability. These findings emphasize the importance of composition and morphology in optimizing the functional properties of PLA/PCL polymer blends for smart and responsive applications. Furthermore, the rheological characterization of PLA/PCL blends is critical for understanding their flow behavior, which directly affects their suitability for additive manufacturing (AM) applications. In extrusion-based AM processes, material properties such as viscosity, phase separation, and crystallization behavior govern the printability, mechanical performance, and interlayer adhesion of fabricated components. By optimizing the rheological properties, this research provides insights into tailoring PLA/PCL blends for eco-friendly and high-performance AM applications.

Author Contributions: Conceptualization, E.I. and R.K.; methodology, E.I., R.K. and V.G.; validation, E.I., V.G., T.B. and V.A.; formal analysis, E.I. and R.K.; investigation, E.I., R.K., V.G. and T.B.; resources, R.K.; data curation, E.I., R.K. and V.G.; writing—original draft preparation, E.I. and R.K.; writing—review and editing, E.I. and R.K.; supervision, E.I. and R.K.; project administration, R.K. All authors have read and agreed to the published version of the manuscript.

Funding: This study was done with the financial support of the European Union—Next GenerationEU within the Project No. BG-RRP-2.011-0001-C01.

Data Availability Statement: The original contributions presented in this study are included in this article. Further inquiries can be directed to the corresponding author.

Conflicts of Interest: The authors declare no conflicts of interest.

References

- Liang, X.; Gao, J.; Xu, W.; Wang, X.; Shen, Y.; Tang, J.; Cui, S.; Yang, X.; Liu, Q.; Yu, L.; et al. Structural mechanics of 3D-printed poly(lactic acid) scaffolds with tetragonal, hexagonal and wheel-like designs. *Biofabrication* **2019**, *11*, 035009. [[CrossRef](#)] [[PubMed](#)]
- Backes, E.H.; Pires, L.D.N.; Beatrice, C.A.G.; Costa, L.C.; Passador, F.R.; Pessan, L.A. Fabrication of biocompatible composites of poly(lactic acid)/hydroxyapatite envisioning medical applications. *Polym. Eng. Sci.* **2020**, *60*, 636–644. [[CrossRef](#)]
- Ivanov, E.; Kotsilkova, R.; Xia, H.; Chen, Y.; Donato, R.K.; Donato, K.; Godoy, A.P.; Di Maio, R.; Silvestre, C.; Cimmino, S.; et al. PLA/Graphene/MWCNT composites with improved electrical and thermal properties suitable for FDM 3D printing applications. *Appl. Sci.* **2019**, *9*, 1209. [[CrossRef](#)]
- Kotsilkova, R.; Ivanov, E.; Georgiev, V.; Ivanova, R.; Menseidov, D.; Batakliiev, T.; Angelov, V.; Xia, H.; Chen, Y.; Bychanok, D.; et al. Essential Nanostructure Parameters to Govern Reinforcement and Functionality of Poly(lactic) Acid Nanocomposites with Graphene and Carbon Nanotubes for 3D Printing Application. *Polymers* **2020**, *12*, 1208. [[CrossRef](#)]
- Silva, T.F.d.; Menezes, F.; Montagna, L.S.; Lemes, A.P.; Passador, F.R. Preparation and characterization of antistatic packaging for electronic components based on poly(lactic acid)/carbon black composites. *J. Appl. Polym. Sci.* **2018**, *136*, 47273. [[CrossRef](#)]
- Scaffaro, R.; Maio, A.; Sutura, F.; Gulino, E.F.; Morreale, M. Degradation and recycling of films based on biodegradable polymers: A short review. *Polymers* **2019**, *11*, 651. [[CrossRef](#)]
- Aydoğdu, M.O.; Altun, E.; Ahmed, J.; Gündüz, O.; Edirisinghe, M. Fiber forming capability of binary and ternary compositions in the polymer system: Bacterial cellulose–polycaprolactone–polylactic acid. *Polymers* **2019**, *11*, 1148. [[CrossRef](#)] [[PubMed](#)]
- Voorde, K.M.V.d.; Pokorski, J.K.; Korley, L.T.J. Exploring morphological effects on the mechanics of blended poly(lactic acid)/poly(ϵ -caprolactone) extruded fibers fabricated using multilayer coextrusion. *Macromolecules* **2020**, *53*, 5047–5055. [[CrossRef](#)]
- Valdés, A.; Dominici, F.; Fortunati, E.; Kenny, J.M.; Jiménez, A.; Garrigós, M.C. Effect of almond skin waste and glycidyl methacrylate on mechanical and color properties of poly(ϵ -caprolactone)/poly(lactic acid) blends. *Polymers* **2023**, *15*, 1045. [[CrossRef](#)]
- Solechan, S.; Suprihanto, A.; Widyanto, S.A.; Triyono, J.; Fitriyana, D.F.; Siregar, J.P.; Cionita, T. Investigating the effect of pcl concentrations on the characterization of pla polymeric blends for biomaterial applications. *Materials* **2022**, *15*, 7396. [[CrossRef](#)]
- Chen, J.; Zhang, T.; Jin, F.; Park, S. Fracture toughness improvement of poly(lactic acid) reinforced with poly(ϵ -caprolactone) and surface--modified silicon carbide. *Adv. Mater. Sci. Eng.* **2018**, *2018*, 6537621. [[CrossRef](#)]
- Ye, G.; Gu, T.; Chen, B.; Bi, H.; Hu, Y. Mechanical, thermal properties and shape memory behaviors of PLA/PCL/PLA-g-GMA blends. *Polym. Eng. Sci.* **2023**, *63*, 2084–2092. [[CrossRef](#)]
- Chomachayi, M.D.; Jalali--Arani, A.; Beltrán, F.R.; Orden, M.U.d.l.; Urreaga, J.M. Biodegradable nanocomposites developed from pla/pcl blends and silk fibroin nanoparticles: Study on the microstructure, thermal behavior, crystallinity and performance. *J. Polym. Environ.* **2020**, *28*, 1252–1264. [[CrossRef](#)]
- Al-Saleh, M.H.; Al-Shboul, T.S. Carbon nanotubes-filled polylactic acid/polycaprolactone biodegradable blends: Effect of the polycaprolactone viscosity and carbon nanotubes addition on the microstructure, electrical and mechanical properties. *J. Thermoplast. Compos. Mater.* **2022**, *36*, 3485–3498. [[CrossRef](#)]
- Khitas, N.; Aouachria, K.; Benaniba, M.T. Blending and plasticising effects on the behaviour of poly(lactic acid)/poly(ϵ -caprolactone). *Polym. Polym. Compos.* **2018**, *26*, 337–345. [[CrossRef](#)]
- Liu, H.; He, H.; Huang, B. Favorable thermoresponsive shape memory effects of 3D printed poly(lactic acid)/poly(ϵ -caprolactone) blends fabricated by fused deposition modeling. *Macromol. Mater. Eng.* **2020**, *305*, 2000295. [[CrossRef](#)]
- Liu, H.; Li, C.; Chen, S.; Chen, P.; Li, J.; Jian, H.; Guo, G.; Chen, X.; Zhu, X.; Wu, J. Fabrication of 3D printed polylactic acid/polycaprolactone nanocomposites with favorable thermo-responsive cyclic shape memory effects, and crystallization and mechanical properties. *Polymers* **2023**, *15*, 1533. [[CrossRef](#)]

18. Urquijo, J.; Dagr eou, S.; Guerrica-Echevarr a, G.; Eguiaz abal, J.I. Structure and properties of poly(lactic acid)/poly(ϵ -caprolactone) nanocomposites with kinetically induced nanoclay location. *J. Appl. Polym. Sci.* **2016**, *133*, 1–11. [[CrossRef](#)]
19. Przybysz-Romatowska, M.; Barczewski, M.; Mania, S.; Tercjak, A.; Haponiuk, J.; Formela, K. Morphology, thermo-mechanical properties and biodegradability of PCL/PLA blends reactively compatibilized by different organic peroxides. *Materials* **2021**, *14*, 4205. [[CrossRef](#)]
20. Luyt, A.S.; Gasmı, S. Influence of blending and blend morphology on the thermal properties and crystallization behaviour of PLA and PCL in PLA/PCL blends. *J. Mater. Sci.* **2016**, *51*, 4670–4681. [[CrossRef](#)]
21. Botlhoko, O.J.; Ramontja, J.; Ray, S.S. A new insight into morphological, thermal, and mechanical properties of meltprocessed poly(lactide)/poly(ϵ -caprolactone) blends. *Polym. Degrad. Stab.* **2018**, *154*, 84–95. [[CrossRef](#)]
22. Shin, B.Y.; Do, H.H. Viscoelastic properties of PLA/PCL blends compatibilized with different methods. *Korea-Aust. Rheol. J.* **2017**, *29*, 295–302. [[CrossRef](#)]
23. Fortelny, I.; Ujci c, A.; Fambri, L.; Slouf, M. Phase Structure, Compatibility, and Toughness of PLA/PCL Blends: A Review. *Front. Mater.* **2019**, *6*, 206. [[CrossRef](#)]
24. Sim oes, C.L.; Viana, J.C.; Cunha, A.M. Mechanical properties of poly (ϵ -caprolactone) and poly (lactic acid) blends. *J. Appl. Polym. Sci.* **2009**, *112*, 345–352. [[CrossRef](#)]
25. Wachirahuttapong, S.; Thongpin, C.; Sombatsompop, N. Effect of PCL and compatibility contents on the morphology, crystallization and mechanical properties of PLA/PCL blends. *Energy Procedia* **2016**, *89*, 198–206. [[CrossRef](#)]
26. Bouakaz, B.S.; Habi, A.; Grohens, Y.; Pillin, I. Organomontmorillonite/graphene-PLA/PCL nanofilled blends: New strategy to enhance the functional properties of PLA/PCL blend. *Appl. Clay Sci.* **2017**, *139*, 81–91. [[CrossRef](#)]
27. Matumba, K.I.; Mokhena, T.C.; Ojijo, V.; Sadiku, E.R.; Ray, S.S. Morphological Characteristics, Properties, and Applications of Poly(lactide)/Poly (ϵ -caprolactone) Blends and Their Composites—A Review. *Macromol. Mater. Eng.* **2024**, *309*, 2400056. [[CrossRef](#)]
28. Garlotta, D.A. Literature Review of Poly(Lactic Acid). *J. Polym. Environ.* **2002**, *9*, 63–84. [[CrossRef](#)]
29. Fischer, E.W.; Sterzel, H.J.; Wegner, G. Investigation of the structure of solution grown crystals of lactide copolymers by means of chemical reactions. *Kolloid-Z. Z. Polym.* **1973**, *251*, 980–990. [[CrossRef](#)]
30. Woodruff, M.A.; Hutmacher, D.W. The return of a forgotten polymer—Polycaprolactone in the 21st century. *Prog. Polym. Sci.* **2010**, *35*, 1217–1256. [[CrossRef](#)]
31. Navarro-Baena, I.; Sessini, V.; Dominici, F.; Torre, L.; Kenny, J.M.; Peponi, L. Design of biodegradable blends based on PLA and PCL: From morphological, thermal and mechanical studies to shape memory behavior. *Polym. Degrad. Stab.* **2016**, *132*, 97–108. [[CrossRef](#)]
32. Ojijo, V.; Ray, S.S.; Sadiku, R. Role of specific interfacial area in controlling properties of immiscible blends of biodegradable poly(lactide) and poly[(butylene succinate)-co-adipate]. *ACS Appl. Mater. Interfaces* **2012**, *4*, 6690–6701. [[CrossRef](#)] [[PubMed](#)]
33. Mittal, V.; Akhtar, T.; Matsko, N. Mechanical, thermal, rheological and morphological properties of binary and ternary blends of PLA, TPS and PCL. *Macromol. Mater. Eng.* **2015**, *300*, 423–435. [[CrossRef](#)]
34. Ostafinska, A.; Fortelny, I.; Nevoralova, M.; Hodan, J.; Kredatusova, J.; Miroslav Slouf, M. Synergistic effects in mechanical properties of PLA/PCL blends with optimized composition, processing, and morphology. *RSC Adv.* **2015**, *5*, 98971–98982. [[CrossRef](#)]
35. Molavi, F.K.; Ghasemi, I.; Messori, M.; Esfandeh, M. Design and characterization of novel potentially biodegradable triple-shape memory polymers based on immiscible poly(l-lactide)/poly(ϵ -caprolactone) blends. *J. Polym. Environ.* **2019**, *27*, 632–642. [[CrossRef](#)]
36. Joshi, M.; Butola, B.S.; Simon, G.; Kukaleva, N. Rheological and viscoelastic behavior of HDPE/cctamethyl-POSS nanocomposites. *Macromolecules* **2006**, *39*, 1839–1849. [[CrossRef](#)]
37. Yeganeh, J.K.; Goharpey, F.; Foudazi, R. Can only rheology be used to determine the phase separation mechanism in dynamically asymmetric polymer blends (PS/PVME). *RSC Adv.* **2012**, *2*, 8116–8127. [[CrossRef](#)]
38. Percoco, G.; Luca Arleo, L.; Stano, G.; Bottiglione, F. Analytical model to predict the extrusion force as a function of the layer height, in extrusion based 3D printing. *Addit. Manuf.* **2021**, *38*, 101791. [[CrossRef](#)]
39. Kotsilkova, R.; Tabakova, S. Exploring effects of graphene and carbon nanotubes on rheology and flow instability for designing printable polymer nanocomposites. *Nanomaterials* **2023**, *13*, 835. [[CrossRef](#)]
40. Ratna, D.; Karger-Kocsis, J. Recent advances in shape memory polymers and composites. A review. *J. Mater. Sci.* **2008**, *43*, 254–269. [[CrossRef](#)]
41. Kazakevi i ut e-Makovska, R.; Mogharebi, S.; Steeb, H.; Eggeler, G.; Neuking, K. A critical assessment of experimental methods for determining the dynamic mechanical characteristics of shape memory polymers. *Adv. Eng. Mat.* **2013**, *15*, 732–739. [[CrossRef](#)]
42. Li, A.; Chen, X.-G.; Zhang, L.-Y.; Zhang, Y.-F. Temperature and infill density effects on thermal, mechanical and shape memory properties of poly(lactic acid)/poly(ϵ -caprolactone) blends for 4D printing. *Materials* **2022**, *15*, 8838. [[CrossRef](#)] [[PubMed](#)]

43. Yong, A.X.; Sims, G.D.; Gnaniyah, S.J.; Ogin, S.L.; Smith, P.A. Heating rate effects on thermal analysis measurement of Tg in composite materials. *Adv. Manuf. Polym. Compos. Sci.* **2017**, *3*, 43–51. [[CrossRef](#)]
44. Curtzwiler, G. The world of surface coatings is centered around the glass transition temperature, but which one? Part 1. *Coat. Tech.* **2014**, *11*, 28–38. Available online: https://www.researchgate.net/publication/279962519_The_world_surface_coatings_is_centerd_around_the_glass_transition_tempraturer_but_which_one_Part_I (accessed on 15 December 2024).
45. O’Neal, H.R.; Welch, S.; Rogers, J.; Guilford, S.; Curran, G.; Menard, K.P.; Rogers, J. Comparison of Tg values for a graphite epoxy composite by differential scanning calorimetry (DSC), thermomechanical analysis (TMA), and dynamic mechanical analysis (DMA). *J. Adv. Mater.* **1995**, *26*, 49–54. Available online: <https://www.semanticscholar.org/paper/Comparisson-of-Tg-values-for-a-graphite-epoxy-by-O’neal-Welch/b8fd883cdcd6a9ea7bd6edb649b12f8a99c294b5> (accessed on 15 December 2024).

Disclaimer/Publisher’s Note: The statements, opinions and data contained in all publications are solely those of the individual author(s) and contributor(s) and not of MDPI and/or the editor(s). MDPI and/or the editor(s) disclaim responsibility for any injury to people or property resulting from any ideas, methods, instructions or products referred to in the content.